

# Numerical evaluation of a two-body point absorber wave energy converter with a tuned inerter

Takehiko Asai<sup>a</sup>, Keita Sugiura<sup>b</sup>

<sup>a</sup>*Faculty of Engineering, Information and Systems, University of Tsukuba, Japan*

<sup>b</sup>*Graduate School of Systems and Information Engineering, University of Tsukuba, Japan*

---

## Abstract

To increase the amount of energy captured from a vibrating buoy in the ocean with a simple mechanism, this paper proposes a two-body point absorber wave energy converter (WEC) with a tuned inerter. The tuned inerter mechanism consists of a spring, a linear damping element, and a component called inerter. This mechanism was originally proposed in the field of civil engineering as a structural control device which can absorb energy from vibrating structures effectively by taking advantage of the resonance effect of the inerter part. In addition to this mechanism where a generator is used as the linear damping element, the current of the generator for the power take-off system is controlled based on the algorithms proposed in literature to achieve further improvement of the power generation capability. In this research, a detailed analytical model of the proposed WEC is introduced and developed. Then the power generation performances of full-scale WEC models are assessed through numerical simulation studies using WAMIT software and it is shown that the current-controlled WEC with the proposed mechanism achieves an 88% increase compared to the conventional one for the JONSWAP spectrum with 6 s peak period and 1 m significant wave height.

*Keywords:* wave energy converter, two-body point absorber, tuned inerter, renewable energy, energy harvesting

---

## 1. Introduction

1 Ocean has been expected to be a promising renewable energy source since  
2 more than 70% of the Earth's surface is covered with oceans. However,  
3 compared with other renewable energy sources such as wind and solar energy,  
4

5 ocean energy conversion technology has not yet shown a strong presence in  
6 the renewable energy market. Since the concept of wave energy converter  
7 (WEC) was introduced by a former Japanese naval commander, Yoshio Ma-  
8 suda (1925-2009) [1], considerable effort has been devoted to develop a variety  
9 of WECs [2, 3, 4, 5] to exploit wave power in the ocean effectively. And vari-  
10 ous types of WECs proposed so far includes oscillating water columns [6, 7],  
11 oscillating bodies [8, 9, 10], and overtopping devices [11, 12, 13]. Among these  
12 devices, point absorbers consisting floating bodies are categorized as the os-  
13 cillating body WEC and more expectations have been placed on this type of  
14 WEC because of its availability in deep offshore regions and its extensibility  
15 by arraying many buoys.

16 To improve the power generation performance of a conventional single-  
17 body point absorber WEC, which has one floating buoy, the authors em-  
18 ployed a tuned inerter mechanism [14, 15]. Originally, the tuned inerter  
19 mechanism was proposed by [16] as a structural control device to absorb  
20 vibration energy effectively from vibrating civil structures such as buildings  
21 induced by seismic disturbances and to mitigate damage. This mechanism  
22 consists of a tuning spring, a linear damping element, and an inerter [17].  
23 The inerter is an element to produce a force proportional to the difference  
24 between the accelerations of both ends and realized by devices such as a ball  
25 screw and a rack and pinion. In the tuned inerter mechanism, the damping  
26 element is installed in parallel with the inerter and these two elements are  
27 connected to the spring in series. Thus, once the spring stiffness is tuned so  
28 that the inerter resonates with the dominant frequency of the input vibra-  
29 tion to the device, the deformation of the damping part is increased and the  
30 vibration energy is dissipated more effectively.

31 The authors employed a generator or a motor as the linear damping  
32 element in the tuned inerter mechanism and showed that the mechanism  
33 enhances the ability to extract energy from vibrating structures at a low  
34 frequency of less than 10 Hz [18, 19]. In addition, the authors proposed a  
35 single-body point absorber WEC with a tuned inerter and the efficacy of  
36 the present device was shown through numerical simulation studies [14] and  
37 wave flume testing using a small-scale prototype model [15].

38 However, generally, the single-body point absorber WEC needs to be  
39 connected directly to the ocean floor. While, a two-body point absorber  
40 WEC [20, 21, 22, 23] consisting of a floating buoy and a submerged body is  
41 just moored, not fixed to the sea bottom. Additionally, the two-body type  
42 has the potential to improve the power generation capability more than the

43 single-body type by designing the two bodies to achieve a greater relative  
 44 velocity between the two bodies.

45 The primary objective of this paper is to propose a two-body point ab-  
 46 sorber WEC with a tuned inerter. A detailed analytical model including  
 47 the coupled force between the two bodies for the proposed WEC and the  
 48 drag force is introduced and the equation of motion and the state-space rep-  
 49 resentation are developed. Then the energy harvesting performance for the  
 50 JONSWAP spectrum is assessed by comparing with a typical two-body point  
 51 absorber WEC without the proposed mechanism. Secondly, the effectiveness  
 52 of the current control of the generator for the power take-off (PTO) system  
 53 of the proposed WEC is investigated. As control algorithms, two controllers  
 54 proposed in [24], i.e., static admittance (SA) control and performance guaran-  
 55 teed (PG) control, are applied to capture more energy. The obtained results  
 56 of the numerical studies using WAMIT [25] are shown and conclusions gained  
 57 from this research follow.

58 It should be noted that we make use of the short-hand  $\mathbf{G} \sim \left[ \begin{array}{c|c} \mathbf{A} & \mathbf{B} \\ \hline \mathbf{C} & \mathbf{D} \end{array} \right]$   
 59 to imply  $\mathbf{G}(s) = \mathbf{C}[s\mathbf{I} - \mathbf{A}]^{-1}\mathbf{B} + \mathbf{D}$  where  $\mathbf{A}$ ,  $\mathbf{B}$ ,  $\mathbf{C}$ , and  $\mathbf{D}$  are the state,  
 60 input, output, and feedthrough matrices of a state-space representation, re-  
 61 spectively, and  $\hat{f}(\omega)$  denotes the Fourier transform of a function  $f(t)$  in this  
 62 article. Also, note that  $j$  is the imaginary unit such that  $j^2 = -1$  and that  
 63 the expected value is denoted by  $\mathcal{E}\{\cdot\}$ .

## 64 2. Modeling

65 To implement numerical studies, the analytical model of the proposed  
 66 WEC is developed here as well as the models of the hydrodynamic forces,  
 67 drag forces, and the JONSWAP spectrum. For simplicity, we consider only  
 68 the heave direction as in the literature [20, 21, 23] because this motion be-  
 69 comes dominant for the power extraction of wave energy. Additionally, the  
 70 generated power is defined in this section. Note that the floating buoy and  
 71 the submerged body are indicated by 1st and 2nd bodies, respectively, in this  
 72 article.

### 73 2.1. Conventional two-body point absorber WEC

74 For comparison, a conventional two-body point absorber WEC consist-  
 75 ing a floating buoy (1st body) and a submerged body (2nd body) shown  
 76 schematically in Fig. 1 (a) is reviewed briefly first. A PTO system including

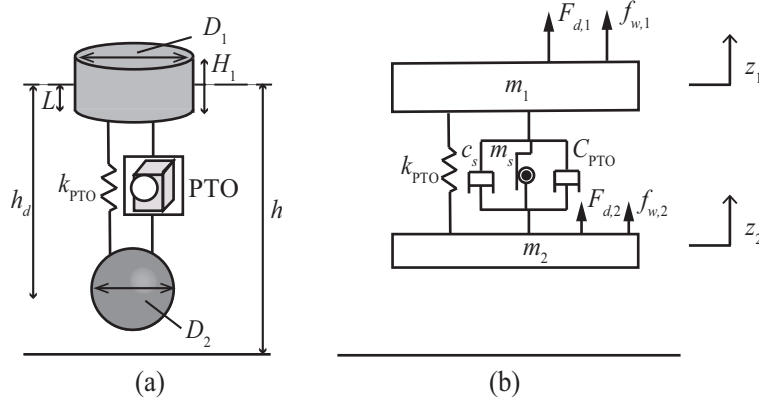


Figure 1: Conventional two-body point absorber WEC: (a) Schematic illustration, (b) Model.

77 a generator is placed between these two bodies. In this research, it is assumed  
 78 that the floating buoy has a circular cylinder shape with a diameter  $D_1$  and  
 79 the submerged body is a sphere with a diameter  $D_2$ . Also, the distance be-  
 80 tween these bodies is  $h_d$  at the static equilibrium position and these bodies  
 81 are connected by a spring whose stiffness is  $k_{\text{PTO}}$ .

82 The model of the conventional type is illustrated in Fig. 1 (b). Let  
 83  $z_k$ , ( $k = 1, 2$ ) be the displacement of the  $k$ th body and  $z_s$  be the rotational  
 84 displacement of the generator. Then we have

$$z_s = z_1 - z_2 \quad (1)$$

85 Hence the equation of motion of the floating buoy would be

$$m_1 \ddot{z}_1 + m_s (\ddot{z}_1 - \ddot{z}_2) + (c_s + C_{\text{PTO}}) (\dot{z}_1 - \dot{z}_2) + k_{\text{PTO}} (z_1 - z_2) = F_{d,1} + f_{w,1} \quad (2)$$

86 where  $m_1$  is the mass of the floating buoy,  $m_s$  is the inertance caused by the  
 87 generator itself,  $c_s$  is the unwanted inherent mechanical damping coefficient  
 88 caused in the PTO system,  $C_{\text{PTO}}$  is the damping coefficient of the generator.  
 89 Also,  $f_{w,1}$  and  $F_{d,1}$  are the hydrodynamic force and the drag force acting on  
 90 the floating buoy, respectively.

91 While, the equation of motion of the submerged body is developed as

$$m_2 \ddot{z}_2 - m_s (\ddot{z}_1 - \ddot{z}_2) - (c_s + C_{\text{PTO}}) (\dot{z}_1 - \dot{z}_2) - k_{\text{PTO}} (z_1 - z_2) = F_{d,2} + f_{w,2} \quad (3)$$

92 where  $m_2$  is the mass of the submerged body and  $f_{w,2}$  and  $F_{d,2}$  are the  
 93 hydrodynamic force and the drag force on the submerged body, respectively,  
 94 similarly to the floating buoy.

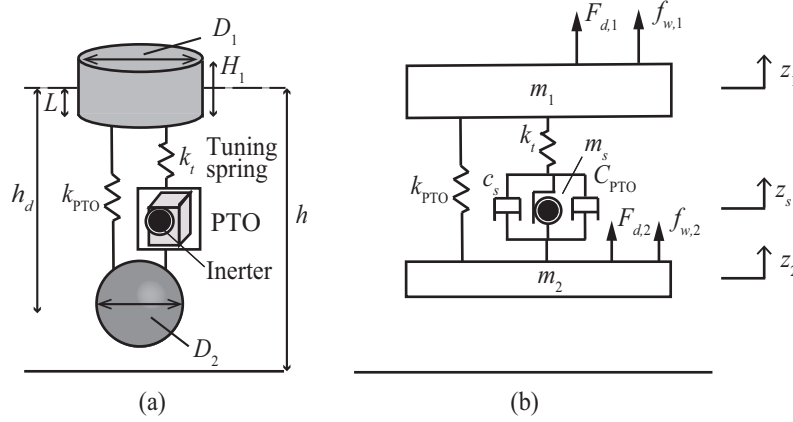


Figure 2: Two-body point absorber WEC with a tuned inerter: (a) Schematic illustration, (b) Model.

95 *2.2. Two-body point absorber WEC with a tuned inerter*

96 Next, the proposed two-body point absorber WEC with a tuned inerter  
 97 shown in Fig. 2 (a) is considered. As can be seen, unlike the conventional two-  
 98 body type, a tuning spring whose stiffness is  $k_t$  is added between the floating  
 99 buoy and the PTO system. Also, an additional rotational mass such as a  
 100 flywheel producing sufficiently large inertance  $m_s$  is mounted intentionally  
 101 on the generator shaft.

102 The model of the present device is shown in Fig. 2 (b) and the equations  
 103 of motion of the device are derived as follows. In contrast to the conventional  
 104 type, Eq. (1) is not satisfied because the proposed system becomes a three-  
 105 degree-of-freedom system due to the tuning spring. Then, for this model, the  
 106 equations of motion of the floating buoy and the submerged body are given  
 107 by

$$108 \quad m_1 \ddot{z}_1 + k_{\text{PTO}}(z_1 - z_2) + k_t(z_1 - z_2 - z_s) = F_{d,1} + f_{w,1} \quad (4)$$

$$109 \quad m_2 \ddot{z}_2 - k_{\text{PTO}}(z_1 - z_2) - k_t(z_1 - z_2 - z_s) = F_{d,2} + f_{w,2} \quad (5)$$

110 respectively. And considering the fact that the force of the tuning spring  
 111 equals the force of the PTO system, the equation of motion of the inerter is  
 derived as

$$m_s \ddot{z}_s + (c_s + C_{\text{PTO}}) \dot{z}_s = k_t(z_1 - z_2 - z_s) \quad (6)$$

112 *2.3. Hydrodynamic force*

113 The hydrodynamic force  $f_{w,k}$  acting on the  $k$ th body is described based  
 114 on the linear potential wave theory by

$$f_{w,k} = f_{a,k} + f_{b,k} + f_{c,k} \quad (7)$$

115 where  $f_{a,k}$  is the excitation force,  $f_{b,k}$  is the hydrodynamic forces due to  
 116 buoyancy, and  $f_{c,k}$  is the radiation force.

117 The relationship between the excitation force  $f_{a,k}$  and the amplitude of  
 118 the incident wave  $a(t)$  is given in the frequency domain using a transfer  
 119 function  $F_{a,k}(\omega)$  as

$$\hat{f}_{a,k}(\omega) = F_{a,k}(\omega)\hat{a}(\omega) \quad (8)$$

120 The hydrostatic force  $f_{b,1}$  on the cylindrical floating buoy becomes a linear  
 121 function of  $z_1$  given as

$$f_{b,1} = -K_w z_1, \quad K_w = \rho g \pi \left( \frac{D_1}{2} \right)^2 \quad (9)$$

122 where  $g$  is gravitational acceleration and  $\rho$  is the sea water density. While  
 123 the hydrostatic force of the submerged body is constant, thus  $f_{b,2}$  can be set  
 124 as

$$f_{b,2} = 0 \quad (10)$$

125 at the equilibrium position in the equation of motion.

126 Next, define  $l = 1, 2, (l \neq k)$ , then the radiation force  $f_{c,k}$  on the  $k$ th body  
 127 including the coupled force affected by the  $l$ th body is given by

$$\hat{f}_{c,k}(\omega) = -(j\omega A_{kk}(\omega) + B_{kk}(\omega))\hat{z}_k - (j\omega A_{kl}(\omega) + B_{kl}(\omega))\hat{z}_l \quad (11)$$

128 where  $A_{kk}$  and  $B_{kk}$  are the added mass and the radiation damping of the  $k$ th  
 129 body, and  $A_{kl}$  and  $B_{kl}$  represent the coupled added mass and the coupled  
 130 radiation damping from the  $l$ th body to the  $k$ th body.

131 *2.4. Drag force*

132 The drag force  $F_{d,k}$  acting on the  $k$ th body is modeled according to the  
 133 nonlinear Morison equation given by [26]

$$F_{d,k} = -\frac{1}{2}\rho S_k C_{d,k} |\dot{z}_k| \dot{z}_k \quad (12)$$

134 where  $S_k$  is the characteristic area and  $C_{d,k}$  is the dimensionless drag coefficient.  
 135 As stated before, in this research, the shapes of the floating buoy and  
 136 the submerged body are assumed to be a cylinder and a sphere, respectively,  
 137 thus we have

$$S_1 = \frac{\pi D_1^2}{4}, \quad S_2 = \frac{\pi D_2^2}{4} \quad (13)$$

138 However, it would be cumbersome to deal with nonlinear equations in  
 139 the frequency domain, Eq. (12) is linearized under the condition of irregular  
 140 wave as [27, 26]

$$F_{d,k} = -\frac{1}{2}\rho S_k C_{d,k} \sqrt{\frac{8}{\pi}} \sigma_{\dot{z}_k} \dot{z}_k \quad (14)$$

141 where  $\sigma_{\dot{z}_k}$  is the standard deviation of  $\dot{z}_k$ . While, in general, the drag force  
 142 of the floating buoy is negligible compared to the hydrodynamic force [28],  
 143 thus we assume that

$$F_{d,1} = 0 \quad (15)$$

144 From, Eq. (14), the linearized drag force on the submerged body is given  
 145 with the viscous damping coefficient  $c_{v,2}$  by

$$F_{d,2} = -c_{v,2} \dot{z}_2, \quad c_{v,2} = \frac{1}{2}\rho S_2 C_{d,2} \sqrt{\frac{8}{\pi}} \sigma_{\dot{z}_2} \quad (16)$$

146 Hereafter, in this article,  $\sigma_{\dot{z}}$  is used to represent the standard deviation of  $\dot{z}_2$   
 147 for simplicity.

### 148 2.5. Stochastic sea state model

149 In simple theoretical models of WECs, it is typical to assume the incident  
 150 waves to be regular. For a more realistic model, irregular waves are used with  
 151 time-domain analysis which requires much more computing time [4]. An  
 152 alternative method with less computation for modeling true sea states is the  
 153 stochastic modeling. We assume the wave amplitude  $a(t)$  to be a stationary  
 154 stochastic process with spectral density  $S_a(\omega)$  which is characterized by the  
 155 JONSWAP spectrum [29] with its mean wave period  $T_1$ , significant wave  
 156 height  $H_s$ , and peak enhancement factor  $\gamma$  expressed as

$$S_a(\omega) = 310\pi \frac{H_s^2}{T_1^4 \omega^5} \exp\left[\frac{-944}{T_1^4 \omega^4}\right] \gamma^W \quad (17)$$

157 where

$$W = \exp \left[ - \left( \frac{0.191\omega T_1 - 1}{\sqrt{2}\sigma} \right)^2 \right], \quad \sigma = \begin{cases} 0.07 & : \omega T_1 \leq 5.24 \\ 0.09 & : \omega T_1 > 5.24 \end{cases} \quad (18)$$

158 The JONSWAP spectrum can also be represented by the peak period  $T_p$   
 159 using the well-known relationship  $T_1 = 0.834T_p$ .

### 160 2.6. Power take-off system

161 In this study, the generator is assumed to be a three-phase permanent  
 162 magnet synchronous machine (PMSM). However, the three phase voltage  
 163 and current vectors can be transformed to "quadrature components". More  
 164 details on this transformation can be found in [24, 30]. Then, assuming an  
 165 ideal generator with linear behavior and minimal core loss results in linearity  
 166 between the back-EMF  $e$  and the velocity coupled with the generator  $\dot{z}_s$ .  
 167 Therefore, the equation relating to  $e$  and  $\dot{z}_s$  is given as

$$e = K_e \dot{z}_s \quad (19)$$

168 where  $K_e$  is a constant associated with the back-EMF of the generator. By  
 169 reciprocity, the electromagnetic force and generator current  $i$  has the follow-  
 170 ing linear relationship

$$C_{\text{PTO}} \dot{z}_s = -K_e i \quad (20)$$

171 In the case of single-directional converter used in [24], the input current  
 172 to the generator  $i$  can be expressed as

$$i = -Y e \quad (21)$$

173 where  $Y$  is the admittance of the generator restricted in ideal conditions by  
 174 [24]

$$Y \in [0, 1/R] \quad (22)$$

175 and  $R$  is the internal or coil resistance of the generator. Applying Eq. (21)  
 176 to Eq. (20) with Eq. (19) yields

$$C_{\text{PTO}} = Y K_e^2 \quad (23)$$

177 which expresses how the generator damping  $C_{\text{PTO}}$  is controlled by the ad-  
 178 mittance  $Y$ .

179 The total power generation is defined as the extracted power minus the  
 180 electrical loss [10]. In this paper, we assume that the current-dependent loss  
 181 is resistive, i.e.,  $Ri^2$ , then we have the power generation as

$$P_g = -ei - Ri^2 \quad (24)$$

182 **3. State-space representation**

183 In this section, to assess the power generation by the current controllers  
 184 under stochastic sea states, a state-space form [31] of the proposed WEC  
 185 augmented with the JONSWAP spectrum is developed. Also, the controllers  
 186 for the current of the generator for power generation are reviewed briefly.

187 *3.1. Two-body point absorber WEC with a tuned inerter*

188 Next, state-space representation for the proposed device is developed here.  
 189 As state-space representation for the conventional two-body WEC can be  
 190 developed in a similar way, its derivation is omitted.

191 Substitute the equations for the hydrodynamic and drag forces into Eqs.  
 192 (4) and (5), then taking Fourier transform gives

$$\begin{aligned} & \{-\omega^2(m_1 + A_{11}(\omega)) + j\omega(c_{v1} + B_{11}(\omega)) + (K_w + k_{PTO} + k_t)\} \hat{z}_1 \\ & + \{-\omega^2 A_{12}(\omega) + j\omega B_{12}(\omega) - (k_{PTO} + k_t)\} \hat{z}_2 \\ & = F_{a,1}(\omega)\hat{a} + k_t\hat{z}_s \end{aligned} \quad (25)$$

193 and

$$\begin{aligned} & \{-\omega^2 A_{21}(\omega) + j\omega B_{21}(\omega) - (k_{PTO} + k_t)\} \hat{z}_1 \\ & + \{-\omega^2(m_2 + A_{22}(\omega)) + j\omega(c_{v2} + B_{22}(\omega)) + (k_{PTO} + k_t)\} \hat{z}_2 \\ & = F_{a,2}(\omega)\hat{a} - k_t\hat{z}_s \end{aligned} \quad (26)$$

194 respectively. Hence, Eqs. (25) and (26) can be combined and written in  
 195 matrix form as

$$\begin{bmatrix} Z_{11} & Z_{12} \\ Z_{21} & Z_{22} \end{bmatrix} \begin{bmatrix} \hat{z}_1 \\ \hat{z}_2 \end{bmatrix} = \begin{bmatrix} F_{a,1} \\ F_{a,2} \end{bmatrix} \hat{a} + \begin{bmatrix} k_t \\ -k_t \end{bmatrix} \hat{z}_s \quad (27)$$

196 where

$$\begin{aligned} Z_{11}(\omega) &= -\omega^2(m_1 + A_{11}(\omega)) + j\omega(B_{11}(\omega)) + (K_w + k_{PTO} + k_t) \\ Z_{12}(\omega) &= -\omega^2 A_{12}(\omega) + j\omega B_{12}(\omega) - (k_{PTO} + k_t) \\ Z_{21}(\omega) &= -\omega^2 A_{21}(\omega) + j\omega B_{21}(\omega) - (k_{PTO} + k_t) \\ Z_{22}(\omega) &= -\omega^2(m_2 + A_{22}(\omega)) + j\omega(c_{v,2} + B_{22}(\omega)) + (k_{PTO} + k_t) \end{aligned} \quad (28)$$

197 Solving Eq. (27) for  $[\hat{z}_1 \ \hat{z}_2]^T$  yields the expressions of form

$$\hat{z}_1 = G_{a,1}(\omega)\hat{a} + G_{z,1}(\omega)\hat{z}_s \quad (29)$$

$$\hat{z}_2 = G_{a,2}(\omega)\hat{a} + G_{z,2}(\omega)\hat{z}_s \quad (30)$$

198 When  $G_{a,1}$ ,  $G_{z,1}$ ,  $G_{a,2}$ , and  $G_{z,2}$  are approximated by finite-dimensional sys-  
 199 tems, we have representations as

$$G_{a,1} \sim \left[ \begin{array}{c|c} \mathbf{A}_{a,1} & \mathbf{B}_{a,1} \\ \hline \mathbf{C}_{a,1} & \mathbf{0} \end{array} \right], \quad G_{z,1} \sim \left[ \begin{array}{c|c} \mathbf{A}_{z,1} & \mathbf{B}_{z,1} \\ \hline \mathbf{C}_{z,1} & \mathbf{0} \end{array} \right] \quad (31)$$

200

$$G_{a,2} \sim \left[ \begin{array}{c|c} \mathbf{A}_{a,2} & \mathbf{B}_{a,2} \\ \hline \mathbf{C}_{a,2} & \mathbf{0} \end{array} \right], \quad G_{z,2} \sim \left[ \begin{array}{c|c} \mathbf{A}_{z,2} & \mathbf{B}_{z,2} \\ \hline \mathbf{C}_{z,2} & \mathbf{0} \end{array} \right] \quad (32)$$

201 It should be noted that the function  $F_{a,k}$  in Eq. (8) is non-causal which will  
 202 be problematic when approximating  $G_{a,1}$  and  $G_{a,2}$  by a finite-dimensional  
 203 state-space. Therefore the technique of spatial delay proposed by Falnes [32]  
 204 is used, defining  $a(t)$  as the wave amplitude at a distance of  $d$  in front of the  
 205 buoy.

206 Once Eqs. (31) and (32) are obtained by system identification techniques,  
 207 the identified systems Eqs. (29) and (30) are represented in the time domain  
 208 as

$$\dot{\mathbf{x}}_1(t) = \mathbf{A}_1 \mathbf{x}_1(t) + \mathbf{G}_1 a(t) + \mathbf{E}_1 z_s(t) \quad (33)$$

$$z_1(t) = \mathbf{C}_1 \mathbf{x}_1(t) \quad (34)$$

209 where  $\mathbf{A}_1$ ,  $\mathbf{G}_1$ ,  $\mathbf{E}_1$ , and  $\mathbf{C}_1$  are expressed by  $\mathbf{A}_{a,1}$ ,  $\mathbf{B}_{a,1}$ ,  $\mathbf{C}_{a,1}$ ,  $\mathbf{A}_{z,1}$ ,  $\mathbf{B}_{z,1}$ , and  
 210  $\mathbf{C}_{z,1}$ . and

$$\dot{\mathbf{x}}_2(t) = \mathbf{A}_2 \mathbf{x}_2(t) + \mathbf{G}_2 a(t) + \mathbf{E}_2 z_s(t) \quad (35)$$

$$z_2(t) = \mathbf{C}_2 \mathbf{x}_2(t) \quad (36)$$

211 where  $\mathbf{A}_2$ ,  $\mathbf{G}_2$ ,  $\mathbf{E}_2$ , and  $\mathbf{C}_2$  are expressed by  $\mathbf{A}_{a,2}$ ,  $\mathbf{B}_{a,2}$ ,  $\mathbf{C}_{a,2}$ ,  $\mathbf{A}_{z,2}$ ,  $\mathbf{B}_{z,2}$ , and  
 212  $\mathbf{C}_{z,2}$  as well.

213 Also, considering  $z_1 - z_2$  as an input, we have a state-space representation  
 214 about the tuned inerter part where the output is the velocity of the generator  
 215 as

$$\dot{\mathbf{x}}_s(t) = \mathbf{A}_s \mathbf{x}_s(t) + \mathbf{B}_s i(t) + \mathbf{E}_s (z_1(t) - z_2(t)) \quad (37)$$

$$\dot{z}_s(t) = \mathbf{C}_s \mathbf{x}_s(t) \quad (38)$$

216 where the state vector is defined as  $\mathbf{x}_s = [z_s \quad \dot{z}_s]^T$  and

$$\mathbf{A}_s = \begin{bmatrix} 0 & 1 \\ -\frac{k_t}{m_s} & -\frac{c_s}{m_s} \end{bmatrix}, \quad \mathbf{B}_s = \begin{bmatrix} 0 \\ \frac{c_e}{m_s} \end{bmatrix}, \quad \mathbf{E}_s = \begin{bmatrix} 0 \\ \frac{k_t}{m_s} \end{bmatrix}, \quad \mathbf{C}_s = [0 \quad 1] \quad (39)$$

217 Define the state vector as  $\mathbf{x}_h = [\mathbf{x}_1^T \ \mathbf{x}_2^T \ \mathbf{x}_s^T]^T$ . Then we have a state-  
 218 space representation in which the inputs are the current  $i$  and the wave height  
 219  $a$  and the output is the voltage  $e$  from Eq. (19) and Eqs. (33) through (39)  
 220 as follows:

$$\dot{\mathbf{x}}_h(t) = \mathbf{A}_h \mathbf{x}_h(t) + \mathbf{B}_h i(t) + \mathbf{G}_h a(t) \quad (40)$$

$$e(t) = \mathbf{C}_h \mathbf{x}_h(t) \quad (41)$$

221 where  $\mathbf{A}_h$ ,  $\mathbf{B}_h$ ,  $\mathbf{G}_h$ , and  $\mathbf{C}_h$  can be composed of  $\mathbf{A}_1$ ,  $\mathbf{A}_2$ ,  $\mathbf{B}_1$ ,  $\mathbf{B}_2$ ,  $\mathbf{G}_1$ ,  $\mathbf{G}_2$ ,  
 222  $\mathbf{C}_1$ ,  $\mathbf{C}_2$ ,  $\mathbf{A}_s$ ,  $\mathbf{B}_s$ ,  $\mathbf{E}_s$ , and  $\mathbf{C}_s$ .

### 223 3.2. JONSWAP spectrum

224 First, a state-space model of the wave amplitude is derived. We find a  
 225 finite-dimensional noise filter

$$F_w \sim \left[ \begin{array}{c|c} \mathbf{A}_w & \mathbf{B}_w \\ \hline \mathbf{C}_w & \mathbf{0} \end{array} \right] \quad (42)$$

226 such that its power spectrum is close to the JONSWAP spectrum, i.e.,  
 227  $S_a(\omega) = |F_w(\omega)|^2$ , for a unit intensity white noise input  $w(t)$ . Then we  
 228 have

$$\dot{\mathbf{x}}_w(t) = \mathbf{A}_w \mathbf{x}_w(t) + \mathbf{B}_w w(t) \quad (43)$$

$$a(t) = \mathbf{C}_w \mathbf{x}_w(t) \quad (44)$$

229 According to the simplified procedure advocated by Spanos [33],  $F_w$  can be  
 230 approximated by a fourth-order controllable canonical form of

$$\mathbf{A}_w = \begin{bmatrix} 0 & 1 & 0 & 0 \\ 0 & 0 & 1 & 0 \\ 0 & 0 & 0 & 1 \\ a_1 & a_2 & a_3 & a_4 \end{bmatrix}, \quad \mathbf{B}_w = \begin{bmatrix} 0 \\ 0 \\ 0 \\ 1 \end{bmatrix}, \quad \mathbf{C}_w = [0 \ 0 \ c_3 \ 0] \quad (45)$$

231 where the filter parameters  $a_1$ ,  $a_2$ ,  $a_3$ ,  $a_4$ , and  $c_3$  are chosen to minimize the  
 232 mean-square error  $\int_{-\infty}^{\infty} (S_a(\omega) - |F_w(\omega)|^2)^2 d\omega$ , while constraining  $a_1$  through  
 233  $a_4$  so that the system poles are in the open left half plane.

234 For example, Fig. 3 shows a JONSWAP spectrum for  $T_p = 6$  s,  $H_s = 1$   
 235 m,  $\gamma = 3.3$  and its fourth-order finite-dimensional approximate system. We  
 236 can confirm in the figure that the fourth-order  $F_w$  estimates the JONSWAP  
 237 spectrum very well. It should be noted that  $H_s = 1$  m,  $\gamma = 3.3$  are fixed in  
 238 the numerical simulation studies in this paper.

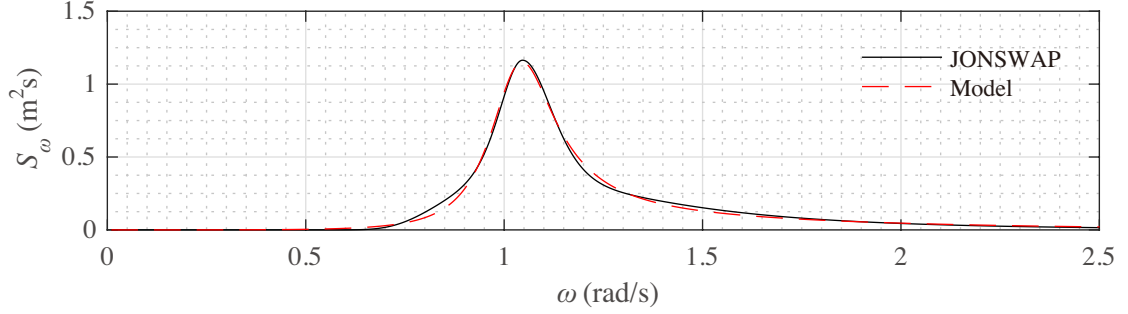


Figure 3: JONSWAP spectrum with  $T_p = 6$  s,  $H_s = 1$  m,  $\gamma = 3.3$

239 *3.3. Augmented system*

240 Finally, combining Eqs. (40) and (41) with the stochastic sea state model  
 241 given by Eqs. (43) and (44) gives the augmented system where the external  
 242 disturbance input is white noise  $w(t)$  expressed as

$$\dot{\mathbf{x}}(t) = \mathbf{A}\mathbf{x}(t) + \mathbf{B}i(t) + \mathbf{G}w(t) \quad (46)$$

$$e(t) = \mathbf{C}\mathbf{x}(t) \quad (47)$$

243 where

$$\mathbf{x} = \begin{bmatrix} \mathbf{x}_h \\ \mathbf{x}_w \end{bmatrix}, \quad \mathbf{A} = \begin{bmatrix} \mathbf{A}_h & \mathbf{G}_h \mathbf{C}_w \\ \mathbf{0} & \mathbf{A}_w \end{bmatrix}, \quad \mathbf{B} = \begin{bmatrix} \mathbf{B}_h \\ \mathbf{0} \end{bmatrix}, \quad \mathbf{G} = \begin{bmatrix} \mathbf{0} \\ \mathbf{B}_w \end{bmatrix}, \quad \mathbf{C} = [\mathbf{C}_h \quad \mathbf{0}] \quad (48)$$

244 *3.4. Controller*

245 To improve the power generation performance and to examine the effec-  
 246 tiveness of the current control on the proposed device, the current of the  
 247 generator  $i$  is controlled by the two control laws introduced in [24] which are  
 248 reviewed briefly here. Before we go any further, it should be noted that the  
 249 average of the generated power defined as Eq. (24) can be written as

$$\bar{P}_g = -\varepsilon \left\{ \begin{bmatrix} \mathbf{x} \\ i \end{bmatrix}^T \begin{bmatrix} \mathbf{0} & \frac{1}{2} \mathbf{C}^T \\ \frac{1}{2} \mathbf{C} & R \end{bmatrix} \begin{bmatrix} \mathbf{x} \\ i \end{bmatrix} \right\} \quad (49)$$

250 using Eq. (47).

251 *3.4.1. Static admittance control*

252 For the SA control, a constant feedback gain  $Y_c$  restricted by Eq. (22) is  
 253 adopted so that the value defined by Eq. (49) is maximized. The method to  
 254 search for such a value is reviewed here.

255 From Eqs. (21) and (47), the input current to the generator is expressed  
 256 as a function of the state variable  $\mathbf{x}$ , i.e.,

$$i(t) = -Y_c \mathbf{C} \mathbf{x}(t) \quad (50)$$

257 Substituting Eq. (50) into Eq. (46) yields the closed-loop dynamics having  
 258 the form

$$\dot{\mathbf{x}}(t) = (\mathbf{A} - Y_c \mathbf{B} \mathbf{C}) \mathbf{x}(t) + \mathbf{G} w(t) \quad (51)$$

259 Let the average power by the SA control be  $\bar{P}_g^{\text{SA}}$ . Then for any time-invariant  
 260  $Y_c$  satisfying Eq. (22), it is a standard result that the power generation  
 261 objective can be written as [34]

$$\bar{P}_g^{\text{SA}} = -\text{tr}[\mathbf{G}^T \mathbf{S} \mathbf{G}] \quad (52)$$

262 where  $\mathbf{S} = \mathbf{S}^T < 0$  is the solution to the Lyapunov equation

$$(\mathbf{A} - Y_c \mathbf{B} \mathbf{C})^T \mathbf{S} + \mathbf{S} (\mathbf{A} - Y_c \mathbf{B} \mathbf{C}) + \mathbf{C}^T (-Y_c + Y_c^2 R) \mathbf{C} = \mathbf{0} \quad (53)$$

263  $Y_c$  must be less than or equal to  $1/R$ , so the last term on the left-hand side  
 264 of Eq. (53) is negative-semidefinite for all  $Y_c$ . Thus, since  $\mathbf{A} - Y_c \mathbf{B} \mathbf{C}$  is  
 265 asymptotically stable, the definiteness of  $\mathbf{S}$  is assured by Lyapunov's second  
 266 theorem [35]. Then the optimal value for  $Y_c$  is chosen so that Eq. (52) is  
 267 maximized.

268 *3.4.2. Performance guaranteed control*

269 For comparison, the efficacy of time-varying gain  $Y$  based on the PG  
 270 control algorithm proposed in the literature is examined. This algorithm is  
 271 operated with a single-directional converter and the admittance  $Y$  becomes  
 272 a function of time varying within the range of Eq. (22) so that the generated  
 273 average power  $\bar{P}_g^{\text{PG}}$  must be larger than  $\bar{P}_g^{\text{SA}}$ , i.e.,

$$\bar{P}_g^{\text{PG}} \geq \bar{P}_g^{\text{SA}} \quad (54)$$

274 In this algorithm, the admittance is controlled by

$$Y(t) = \underset{[0, 1/R]}{\text{sat}} \left\{ \frac{\mathbf{K} \mathbf{x}}{e} \right\} \quad (55)$$

275 where

$$\mathbf{K} = -\frac{1}{R} \left( \mathbf{B}^T \mathbf{S} + \frac{1}{2} \mathbf{C} \right) \quad (56)$$

276 Note that  $Y_c$  is the constant value for the SA control. In this case, the current  
277  $i$  is expressed by

$$i(t) = \begin{cases} i_u(t) & : i_u e + i_u^2 R \leq 0 \\ 0 & : i_u e + i_u^2 R > 0 \text{ and } i_u e > 0 \\ -e(t)/R & : \text{otherwise} \end{cases} \quad (57)$$

278 where

$$i_u = \mathbf{K} \mathbf{x} \quad (58)$$

279 And the generated average energy would be

$$\bar{P}_g^{\text{PG}} = \bar{P}_g^{\text{SA}} + R \mathcal{E} \{ (i_u + Y_c e)^2 - (i_u - i)^2 \} \quad (59)$$

280 which guarantees the inequality given by Eq. (54).

## 281 4. Numerical simulation

282 To verify the efficacy of the proposed two-body point absorber WEC, nu-  
283 merical simulation studies are carried out in this section. First, the paramete-  
284 rer values of the model used here are developed, then the power generation  
285 performance is assessed.

### 286 4.1. Model development

287 The parameter values for the two-body point absorber used here is deter-  
288 mined based on the study conducted in [20], which are summarized in Table  
289 1.

290 The added mass and the radiation damping of the floating buoy and  
291 the submerged body calculated using WAMIT software [25] are shown in  
292 Figs. 4 and 5, respectively. The magnitude and the phase of the transfer  
293 functions given by Eq. (8) are shown in the figures as well. Moreover, the  
294 coupled added mass and radiation damping acting on the floating buoy from  
295 the submerged body, i.e.,  $A_{12}$  and  $B_{12}$  and vice versa, i.e.,  $A_{21}$  and  $B_{21}$  are  
296 shown in Fig. 6.

297 Then, from Eqs. (27) and (28), the frequency response data for  $G_{a,1}$ ,  $G_{z,1}$ ,  
298  $G_{a,2}$ , and  $G_{z,2}$  in Eqs. (29) and (30) are calculated as depicted in Figs. 7 and

Table 1: Parameter values for numerical simulation

Parameter	Value	Parameter	Value
$m_1$	58,075 kg	$m_2$	34,515 kg
$D_1$	6.0 m	$D_2$	4.0 m
$H_1$	2.5 m	$L$	2.0 m
$h$	400 m	$h_d$	20 m
$k_t$	10,000 N/m	$k_{\text{PTO}}$	100,000 N/m
$c_s$	50 Ns/m	$C_{d,2}$	0.1
$R$	25 $\Omega$	$\rho$	1,027 kg/m <sup>3</sup>

299 8 by solid lines. Then, to express these in state-space form as expressed by  
300 Eqs. (31) and (32),  $G_{a,1}$  and  $G_{a,2}$  are approximated with 5 zeros and 6 poles,  
301 and  $G_{z,1}$  with 2 zeros and 4 poles, and  $G_{z,2}$  with 4 zeros and 5 poles. These  
302 numbers are chosen by trial and error so that the finite-dimensional models  
303 shown by dashed lines approximate the frequency response data very well.  
304 This derivation is carried out using MATLAB [36] in this research. Note that  
305 the wave amplitude  $a(t)$  is taken to be the wave amplitude  $d = 10$  m ahead  
306 of the buoy in the propagation direction.

#### 307 4.2. Inerter design

308 Next, the inertance  $m_s$  for the proposed WEC needs to be designed. In  
309 this study, this value is chosen so that the average power generation for the  
310 JONSWAP spectrum with  $T_p = 6$  s is maximized when the SA controller is  
311 applied. While the damping coefficient of the drag force on the submerged  
312 body given by (16) depends on the standard deviation of the velocity  $\dot{z}_2$ .  
313 Thus, the value  $m_s$  is designed according to the flowchart as shown in Fig.  
314 9 (a) here, in which  $\sigma_{\dot{z}_2^-}$  and  $\sigma_{\dot{z}_2}$  are standard deviations at the previous and  
315 current iterations, respectively. This flowchart is made based on the method  
316 to determine  $\sigma_{\dot{z}_2}$  introduced in [26]. For this iteration process, the initial value  
317 for  $\sigma_{\dot{z}_2}$  is set to  $\sigma_{\dot{z}_2 0} = 0.1$  m/s and the range for  $m_s$  is set between  $m_{s0} = 5,000$   
318 kg and  $m_{se} = 10,000$  kg and the best value is sought with respect to each  
319 100 kg iteratively.

320 During the iteration, the standard deviation of  $\dot{z}_2$  is calculated simply  
321 from

$$\sigma_{\dot{z}_2}^2 = \mathbf{G}^T \mathbf{S}_z \mathbf{G} \quad (60)$$

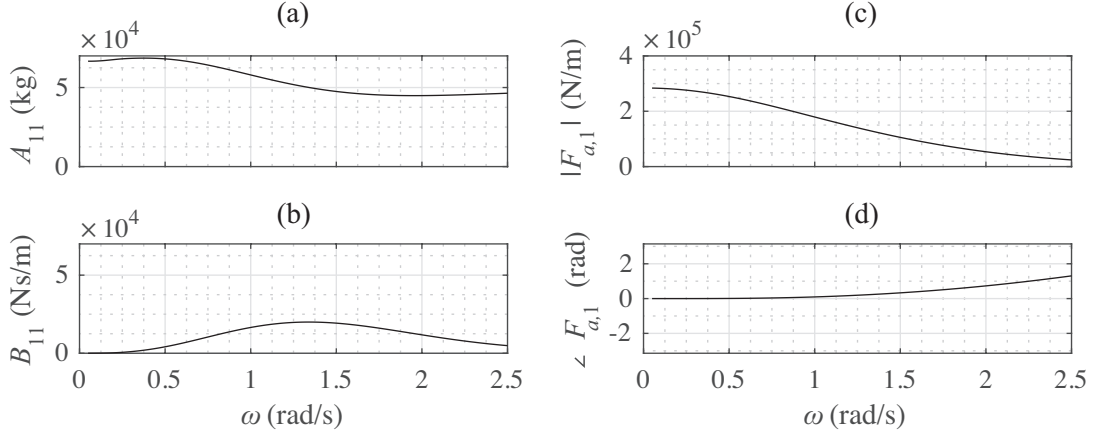


Figure 4: Hydrodynamic parameters for the heave mode of the floating buoy : (a) Added mass  $A_{11}$ , (b) Radiation damping  $B_{11}$ , (c) Magnitude of  $F_{a,1}(\omega)$ , (d) Phase of  $F_{a,1}(\omega)$ .

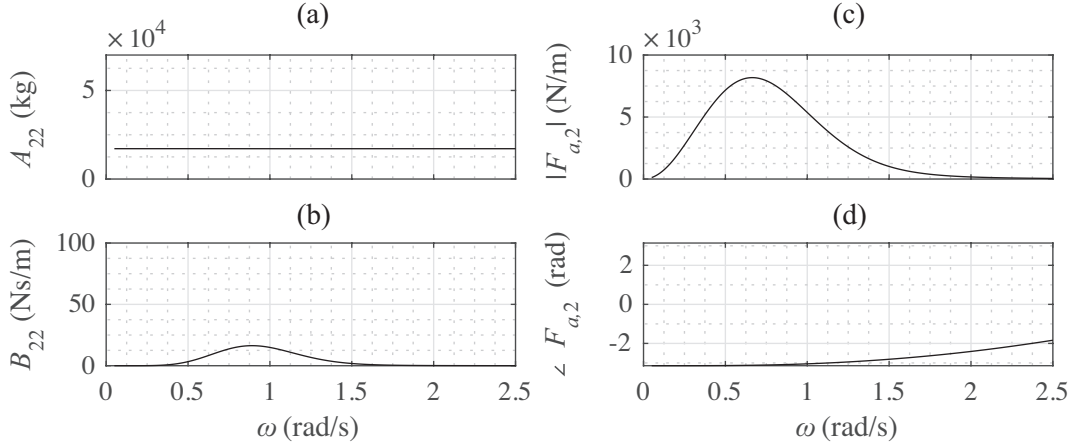


Figure 5: Hydrodynamic parameters for the heave mode of the submerged body : (a) Added mass  $A_{22}$ , (b) Radiation damping  $B_{22}$ , (c) Magnitude of  $F_{a,2}(\omega)$ , (d) Phase of  $F_{a,2}(\omega)$ .

322 where  $\mathbf{S}_z = \mathbf{S}_z^T > 0$  is the solution to the Lyapunov equation

$$(\mathbf{A} - Y_c \mathbf{B} \mathbf{C})^T \mathbf{S}_z + \mathbf{S}_z (\mathbf{A} - Y_c \mathbf{B} \mathbf{C}) + \mathbf{C}_z^T \mathbf{C}_z = \mathbf{0} \quad (61)$$

323 and

$$\dot{z}_2 = \mathbf{C}_z \mathbf{x} \quad (62)$$

324 Then, if the difference between the obtained  $\sigma_z$  and the previous value  $\sigma_z^-$   
 325 is larger than 0.001, the damping coefficient for the linearized drag force is

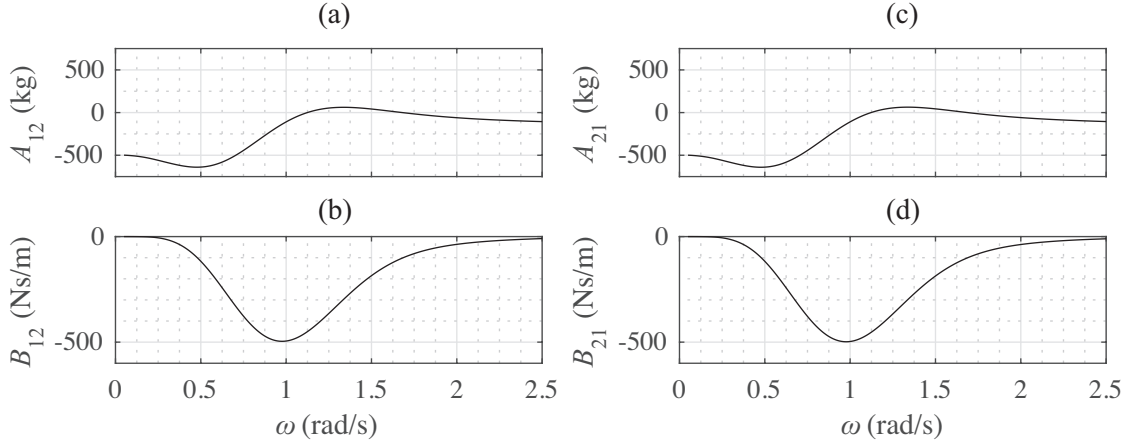


Figure 6: Coupled hydrodynamic parameters for the heave mode of the two bodies : (a) Added mass,  $A_{12}$  (b) Radiation damping  $B_{12}$ , (c) Added mass  $A_{21}$ , (d) Radiation damping  $B_{21}$ .

326 recalculated using the newly obtained  $\sigma_{\dot{z}}$  from Eq. (16). This procedure  
 327 continues until the value of the standard deviation converges enough. And  
 328 the average power for the SA control is calculated using the converged  $\sigma_{\dot{z}}$   
 329 from Eq. (52)

330 The average power obtained in the process of the flowchart is plotted in  
 331 Fig. 10. As can be seen, the generation performance peaks at  $m_s = 6,900$   
 332 kg, which is used for the numerical simulation studies.

### 333 4.3. Drag force model

334 The damping coefficient  $c_{v,2}$  for the linearized drag force acting on the  
 335 submerged body as expressed by Eq. (16) still needs to be obtained for  
 336 each peak wave period  $T_p$ . The inertance value is set to  $m_s = 6,900$  kg as  
 337 determined before. Then we seek for the damping coefficient value for each  
 338  $T_p$  of the JONSWAP spectrum based on the flowchart shown in Fig. 9 (b).  
 339 This is referred to the flowchart in [26] as well as Fig. 9 (a). For the process,  
 340  $\sigma_{\dot{z}}$  is first set to  $\sigma_{\dot{z}0} = 0.1$  m/s as well as before and  $c_{v,2}$  is investigated in  
 341 the range of the peak wave period  $T_p$  from 2 s and 12 s, i.e., we set  $T_{p0} = 2$   
 342 s and  $T_{pe} = 12$  s.

343 The result for the case of the two-body point absorber with a tuned inerter  
 344 of  $m_s = 6,900$  kg is shown in Fig. 11. We can find that  $c_{v,2}$  is much larger  
 345 than the radiation damping on the submerged body denoted by  $B_{22}$  and  
 346 confirm that the drag force on the submerged body should not be ignored.

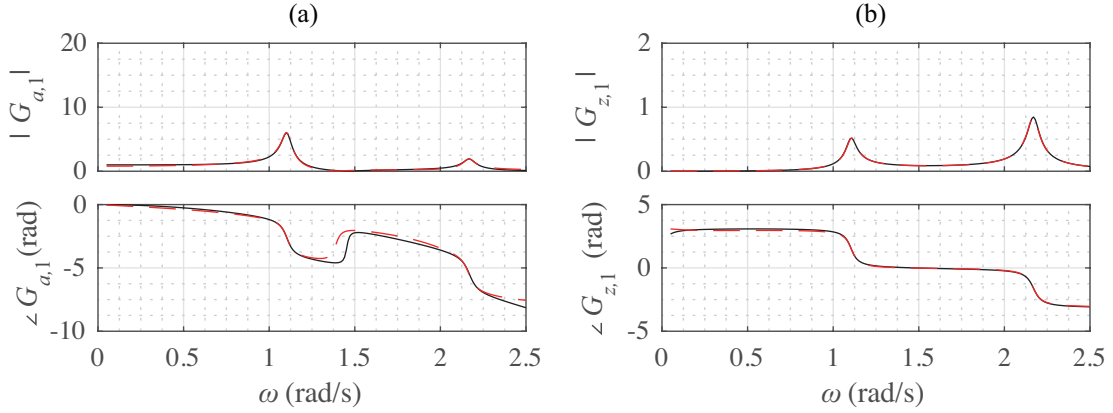


Figure 7: Frequency domain data (solid) and finite-dimensional approximation (dashed) :  
(a)  $G_{a,1}(\omega)$  , (b)  $G_{z,1}(\omega)$ .

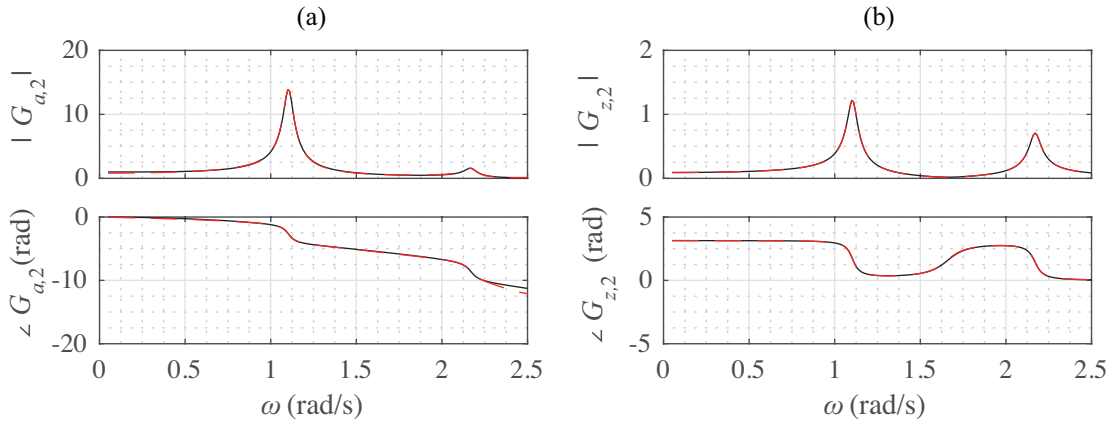


Figure 8: Frequency domain data (solid) and finite-dimensional approximation (dashed) :  
(a)  $G_{a,2}(\omega)$  , (b)  $G_{z,2}(\omega)$ .

#### 347 4.4. Results

348 Finally, the average power generations for the JONSWP spectrum with  
349 the peak wave period from 2 s to 12 s are calculated from the parameter values  
350 determined above. The results obtained from the SA and the PG controllers  
351 are compared in Fig. 12 (a), in which the proposed point absorber WEC with  
352 a tuned inerter and the conventional WEC cases are denoted by 2BwTI and  
353 2B, respectively. The average power for the SA control cases can be given by  
354 the closed form expressed by Eq. (52), however, for consistency with the PG  
355 control cases, the average values shown in Fig. 12 (a) are calculated from Eq.

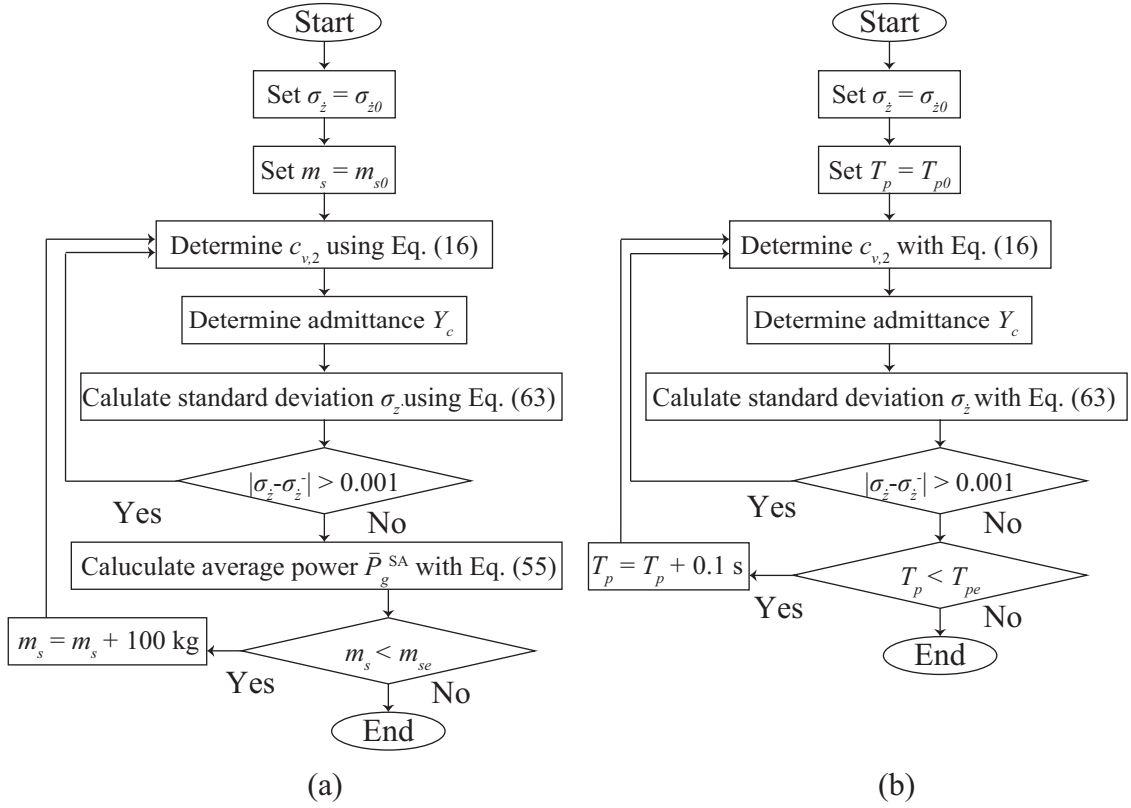


Figure 9: Flowchart: (a) Inerter design, (b) Drag force model.

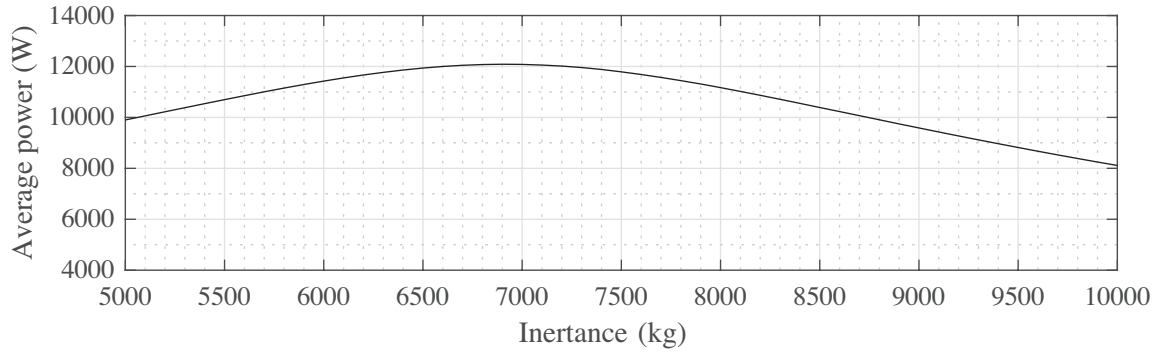


Figure 10: Average power vs inerter.

356 (24) using the numerical simulation results for 100,000 s. The admittances for  
 357 the SA controller are compared in Fig. 12 (b) which shows the difference of

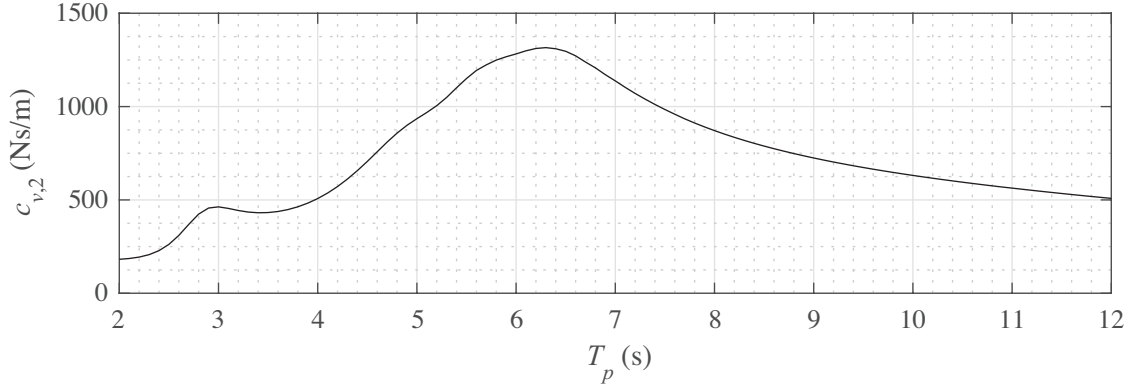


Figure 11: Damping coefficient  $c_{v,2}$  for the drag force on the submerged body.

358 the optimized admittance between the proposed and the conventional WECs.  
 359 For the assessment of the conventional WEC, the same parameters as the  
 360 proposed WEC are employed except that  $m_s = 50$  kg. As you can see in Fig.  
 361 12 (a), the proposed WEC shows the better power generation performance  
 362 than the conventional WEC in the wide range of the peak wave period  $T_p$  even  
 363 though the effectiveness deteriorates in a certain range of the lower period.  
 364 Especially, the superiority of the proposed WEC is notable around  $T_p = 6$  s  
 365 to which the inerter of the proposed WEC is designed to be tuned. Also, the  
 366 PG controller works well to improve the power generation especially for the  
 367 proposed WEC. Specifically, the calculated average powers of 2B-SA, 2B-PG,  
 368 2BwTI-SA, and 2BwTI-PG cases when  $T_p = 6$  s are 7,180 W, 7706 W, 12,030  
 369 W, and 13530 W, respectively. Thus, the present WEC controlled based on  
 370 the PG algorithm achieves an 88% increase compared to the conventional  
 371 WEC.

#### 372 4.5. Discussion

373 It is shown through the numerical simulation studies that the tuned inerter  
 374 mechanism works well on the two-body point absorber WEC. However,  
 375 to enhance the credibility of the device, more elaborate studies employing a  
 376 more accurate model considering non-linearity and behaviors other than the  
 377 heave direction are necessary. Also, the optimum design for the shapes of the  
 378 floating buoy and the submerged body should be examined more thoroughly  
 379 and it is worth trying other simulation schemes, for example, a CFD (com-  
 380 putational fluid dynamics) technique and WEC-SIM [37]. Moreover, various

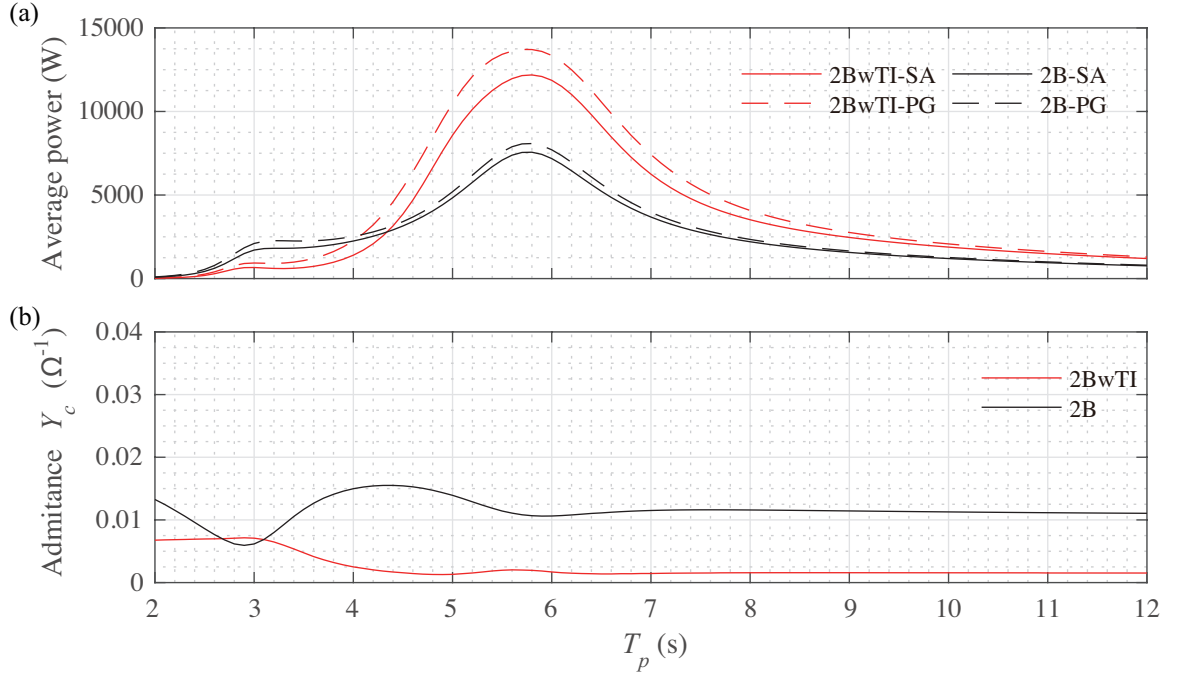


Figure 12: Results. (a) Power generation, (b) Admittance.

381 control algorithms such as reactive controllers should be applied to the gen-  
 382 erator current of the proposed WEC or more effective controllers need to be  
 383 developed. For a practical perspective, experimental verification is still desir-  
 384 able and the capture width ratio and the levelized cost of electricity (LCOE)  
 385 of the present device should be calculated and compared to other devices.

## 386 5. Conclusions

387 This article introduced the two-body point absorber WEC with a tuned  
 388 inerter and developed the detailed analytical model including the coupled  
 389 force between the two bodies. Then, its effectiveness was verified by compar-  
 390 ing the conventional two-body point absorber WEC through the numerical  
 391 simulation studies using the values obtained from WAMIT software. The re-  
 392 sults for the JONSWAP spectrum showed that the tuned inerter mechanism  
 393 not only increased the power generation performance but also broadened the  
 394 effective range of the peak period of the JONSWAP spectrum. Moreover,  
 395 this research showed that the performance of the proposed WEC was im-

396 proved further by controlling the current of the generator. Considering the  
397 results obtained in this research, we conclude that the tuned inerter mech-  
398 anism has great potential to improve the power generation performance of  
399 the two-body point absorber WEC.

#### 400 **Acknowledgments**

401 The authors gratefully acknowledge support for this research through  
402 JSPS KAKENHI Grant number 18K189808 and TEPCO (Tokyo Electric  
403 Power Company) Memorial Foundation.

#### 404 **References**

- 405 [1] Y. Masuda, An experience of wave power generator through tests and  
406 improvement, in: D. V. Evans, A. F. O. de Falcão (Eds.), *Hydrody-*  
407 *namics of Ocean Wave-Energy Utilization*, Springer Berlin Heidelberg,  
408 Berlin, Heidelberg, 1986, pp. 445–452.
- 409 [2] M. McCormick, *Ocean Wave Energy Conversion*, Dover Civil and Me-  
410 *chanical Engineering Series*, Dover Publications, 2007.
- 411 [3] J. Falnes, A review of wave-energy extraction, *Marine Structures* 20 (4)  
412 (2007) 185 – 201. doi:<https://doi.org/10.1016/j.marstruc.2007.09.001>.
- 413 [4] A. F. de O. Falcão, Wave energy utilization: A review of the technolo-  
414 gies, *Renewable and Sustainable Energy Reviews* 14 (3) (2010) 899 –  
415 918. doi:<https://doi.org/10.1016/j.rser.2009.11.003>.
- 416 [5] E. Rusu, F. Onea, A review of the technologies for wave energy extrac-  
417 tion, *Clean Energy* 2 (1) (2018) 10–19. doi:[10.1093/ce/zky003](https://doi.org/10.1093/ce/zky003).
- 418 [6] A. F. Falcão, J. C. Henriques, Oscillating-water-column wave energy  
419 converters and air turbines: A review, *Renewable Energy* 85 (2016)  
420 1391 – 1424. doi:<https://doi.org/10.1016/j.renene.2015.07.086>.
- 421 [7] D. V. EVANS, The Oscillating Water Column Wave-energy De-  
422 vice, *IMA Journal of Applied Mathematics* 22 (4) (1978) 423–433.  
423 doi:[10.1093/imamat/22.4.423](https://doi.org/10.1093/imamat/22.4.423).
- 424 [8] K. Budar, J. Falnes, A resonant point absorber of ocean-wave power,  
425 *Nature* 256 (5517) (1975) 478.

- 426 [9] J. Falnes, *Ocean Waves and Oscillating Systems: Linear Interactions*  
427 *Including Wave-Energy Extraction*, Cambridge University Press, 2002.  
428 doi:10.1017/CBO9780511754630.
- 429 [10] J. Scruggs, S. Lattanzio, A. Taflanidis, I. Cassidy, Optimal causal control  
430 of a wave energy converter in a random sea, *Applied Ocean Research* 42  
431 (2013) 1 – 15. doi:https://doi.org/10.1016/j.apor.2013.03.004.
- 432 [11] P. Contestabile, G. Crispino, E. Di Lauro, V. Ferrante, C. Gissoni,  
433 D. Vicinanza, Overtopping breakwater for wave energy con-  
434 version: Review of state of art, recent advancements and  
435 what lies ahead, *Renewable Energy* 147 (2020) 705 – 718.  
436 doi:https://doi.org/10.1016/j.renene.2019.08.115.
- 437 [12] L. Margheritini, D. Vicinanza, P. Frigaard, Ssg wave energy con-  
438 verter: Design, reliability and hydraulic performance of an innova-  
439 tive overtopping device, *Renewable Energy* 34 (5) (2009) 1371 – 1380.  
440 doi:https://doi.org/10.1016/j.renene.2008.09.009.
- 441 [13] J. P. Kofoed, P. Frigaard, E. Friis-Madsen, H. C. Sørensen,  
442 Prototype testing of the wave energy converter wave dragon,  
443 *Renewable Energy* 31 (2) (2006) 181 – 189, *marine Energy*.  
444 doi:https://doi.org/10.1016/j.renene.2005.09.005.
- 445 [14] R. Haraguchi, T. Asai, Enhanced power absorption of a point absorber  
446 wave energy converter using a tuned inertial mass, *Energy* 202 (2020)  
447 117740. doi:https://doi.org/10.1016/j.energy.2020.117740.
- 448 [15] K. Sugiura, R. Sawada, Y. Nemoto, R. Haraguchi, T. Asai,  
449 Wave flume testing of an oscillating-body wave energy converter  
450 with a tuned inerter, *Applied Ocean Research* 98 (2020) 102127.  
451 doi:https://doi.org/10.1016/j.apor.2020.102127.
- 452 [16] K. Ikago, K. Saito, N. Inoue, Seismic control of single-degree-of-freedom  
453 structure using tuned viscous mass damper, *Earthquake Engineering &*  
454 *Structural Dynamics* 41 (3) 453–474. doi:10.1002/eqe.1138.
- 455 [17] M. C. Smith, Synthesis of mechanical networks: The inerter, *Proceed-*  
456 *ings of the IEEE Conference on Decision and Control* 2 (10) (2002)  
457 1657–1662. doi:10.1109/cdc.2002.1184758.

- 458 [18] T. Asai, Y. Araki, K. Ikago, Energy harvesting potential  
459 of tuned inertial mass electromagnetic transducers, *Mechan-*  
460 *ical Systems and Signal Processing* 84 (2017) 659 – 672.  
461 doi:<https://doi.org/10.1016/j.ymssp.2016.07.048>.
- 462 [19] K. Sugiura, Y. Watanabe, T. Asai, Y. Araki, K. Ikago, Experimental  
463 characterization and performance improvement evaluation of an electro-  
464 magnetic transducer utilizing a tuned inerter, *Journal of Vibration and*  
465 *Control* 26 (1-2) (2020) 56–72. doi:[10.1177/1077546319876396](https://doi.org/10.1177/1077546319876396).
- 466 [20] E. A. Shami, X. Wang, R. Zhang, L. Zuo, A parameter study and op-  
467 timization of two body wave energy converters, *Renewable Energy* 131  
468 (2019) 1 – 13. doi:<https://doi.org/10.1016/j.renene.2018.06.117>.
- 469 [21] D. Martin, X. Li, C.-A. Chen, K. Thiagarajan, K. Ngo, R. Parker,  
470 L. Zuo, Numerical analysis and wave tank validation on the optimal  
471 design of a two-body wave energy converter, *Renewable Energy* 145  
472 (2020) 632 – 641. doi:<https://doi.org/10.1016/j.renene.2019.05.109>.
- 473 [22] E. Anderlini, D. Forehand, E. Bannon, Q. Xiao, M. Abusara,  
474 Reactive control of a two-body point absorber using rein-  
475 forcement learning, *Ocean Engineering* 148 (2018) 650 – 658.  
476 doi:<https://doi.org/10.1016/j.oceaneng.2017.08.017>.
- 477 [23] X. Li, D. Martin, C. Liang, C. Chen, R. G. Parker, L. Zuo,  
478 Characterization and verification of a two-body wave energy  
479 converter with a novel power take-off, *Renewable Energy*—  
480 doi:<https://doi.org/10.1016/j.renene.2020.08.113>.
- 481 [24] I. L. Cassidy, J. T. Scruggs, Nonlinear stochastic controllers  
482 for power-flow-constrained vibratory energy harvesters, *Jour-*  
483 *nal of Sound and Vibration* 332 (13) (2013) 3134 – 3147.  
484 doi:<https://doi.org/10.1016/j.jsv.2013.01.023>.
- 485 [25] WAMIT, Inc., WAMIT, <http://www.wamit.com/index.htm>, MA, USA  
486 (2020).
- 487 [26] C. O. Housseine, C. Monroy, G. de Hauteclocque, Stochastic Lineariza-  
488 tion of the Morison Equation Applied to an Offshore Wind Turbine, in:  
489 Volume 9: Ocean Renewable Energy, American Society of Mechanical  
490 Engineers, 2015. doi:[10.1115/OMAE2015-41301](https://doi.org/10.1115/OMAE2015-41301).

- 491 [27] N. H. Thinh, N. D. Anh, D. A. Cuong, An equivalent linearization for  
492 the drag force in the Morison's equation using Hermite polynomial error  
493 sample function, *Vietnam Journal of Mechanics* 20 (2) (1998) 55–64.  
494 doi:10.15625/0866-7136/10021.
- 495 [28] B. Guo, R. Patton, S. Jin, J. Gilbert, D. Parsons, Nonlinear modeling  
496 and verification of a heaving point absorber for wave energy conver-  
497 sion, *IEEE Transactions on Sustainable Energy* 9 (1) (2018) 453–461.  
498 doi:10.1109/TSTE.2017.2741341.
- 499 [29] O. Faltinsen, *Sea Loads on Ships and Offshore Structures*, Cambridge  
500 Ocean Technology Series, Cambridge University Press, 1993.
- 501 [30] R. R. Krishnan, *Electric motor drives : modeling, analysis, and control*,  
502 Upper Saddle River, N.J. : Prentice Hall, 2001, includes bibliographical  
503 references and index.
- 504 [31] W. Brogan, *Modern Control Theory*, Prentice Hall, 1991.
- 505 [32] J. Falnes, On non-causal impulse response functions related to prop-  
506 agating water waves, *Applied Ocean Research* 17 (6) (1995) 379–389.  
507 doi:10.1016/S0141-1187(96)00007-7.
- 508 [33] P.-T. Spanos, Filter approaches to wave kinematics ap-  
509 proximation, *Applied Ocean Research* 8 (1) (1986) 2 – 7.  
510 doi:https://doi.org/10.1016/S0141-1187(86)80025-6.
- 511 [34] P. Dorato, C. Abdallah, V. Cerone, *Linear Quadratic Control: An In-*  
512 *troduction*, Krieger Publishing Company, 1995.
- 513 [35] R. Stengel, *Optimal Control and Estimation*, Dover books on advanced  
514 mathematics, Dover Publications, 1986.
- 515 [36] MathWorks, MATLAB, <https://www.mathworks.com/>, MA, USA  
516 (2020).
- 517 [37] M. J. Lawson, Y. Yu, K. Ruehl, C. Michelen, Development and demon-  
518 stration of the wec-sim wave energy converter simulation tool, in: *Pro-*  
519 *ceedings of the 2nd Marine Energy Technology Symposium, METS,*  
520 2014.